JOURNAL OF PROPULSION AND POWER
Vol. 17, No. 3, May–June 2001

Stress and Buckling Analyses of Multitube, Vapor-Anode, Nb-1Zr/C-103 AMTEC Cells

Jeffrey C. King* and Mohamed S. El-Genk†
University of New Mexico, Albuquerque, New Mexico 87131

Linear stress and buckling analyses of Nb-1Zr/C-103 AMTEC cells, mounted in a radioisotope generator configuration, are performed using finite element analysis software. The stress analyses indicated that the total induced Von Mises stresses in the structural support members of the cells will not exceed 86% of the temperature-dependent yield stresses of their respective materials. The buckling analyses indicated the need to add ribs to reinforce the cell wall and to decrease the pressure of the inert cover gas present in the generator during launch to 125 kPa. The total mass of the ribbed Nb-1Zr/C-103 cell is 171.5 g, and its specific mass at the predicted maximum electric power of 8.0 W_e is 21.3 g/W_e.

Introduction

AN AMTEC cell is a thermal-to-electric conversion device in which electric potential is produced as a result of the isothermal expansion of sodium ions through beta-alumina solid electrolyte (BASE). BASE is a solid ceramic material with high sodium-ion conductivity and very low electron conductivity. A typical multitube, vapor-anode AMTEC cell (Fig. 1) consists of 5–9 BASE tubes connected electrically in series to provide a load voltage of at least 3.0 V per cell. The BASE tubes are electrically insulated from each other and from the support plate using a metal-ceramic braze structure (Fig. 1), which is thermally conductive, but electrically insulating.

The AMTEC cell consists of two enclosures (see Fig. 1): The high-pressure enclosure, in which the sodium vapor pressure is about 60 kPa, and the low-pressure enclosure, in which the sodium vapor pressure is ~20–40 Pa. The thickness of the cell wall above the BASE (~100 μm) is almost half that of the wall facing the BASE tubes in order to reduce conduction losses.

Several stainless-steel AMTEC cells have been tested in vacuum; and some have operated continuously for more than 8000 h without failure, but with appreciable degradation in performance,[1–3] possibly as a result of mass transport of volatile alloying elements from stainless steel and/or degradation of the TiN electrodes covering the BASE. In an attempt to replace the stainless-steel structure, El-Genk et al. performed parametric analyses of a nickel/Haynes-25 AMTEC cell similar in design to that shown in Fig. 2. (Ref. 4). However, because of concerns regarding the solubility of nickel in liquid sodium and the volatility of chromium at high temperatures, attention focused on replacing both nickel and Haynes-25 (which contains up to 20 atom% chromium) with refractory alloys.[5]

A Nb-1Zr cell has been proposed that has a predicted power of 8.94 W_e at 3.5 V and 16.4% conversion efficiency.[6] Recently, El-Genk and King designed and analyzed the performance of a Nb-1Zr/C-103 cell (Fig. 2), which has a predicted maximum power of 8.3 W_e at 3.0 V and an efficiency of 17.3%; the corresponding specific mass of the cell was 19.7 g/W_e (Ref. 7). At a load voltage of 3.5 V, the cell power was 7.97 W_e, but the efficiency was higher (18.4%), providing a specific mass of 20.5 g/W_e.

Although considerable work has been documented on the design and performance of AMTEC cells, very little has been reported on the structural analyses of these cells during launch. Hendricks et al. performed a stress analysis of a radioisotope power generator (see Fig. 3) with two GPHS modules and 16 stainless-steel AMTEC cells; however, in these analyses, neither the temperatures nor the cell operating conditions used were reported.[8] The predicted maximum stress (508 MPa) was in the zirconia/titanium load studs (see Fig. 3), and the highest predicted stress in the AMTEC cells was 177 MPa. The results noted the importance of allowing for radial and axial thermal expansion of the cells in the generator in order to prevent excessive thermal stresses; however, details of the thermal stress analyses were not provided.[8]

Ruhkamp et al. investigated the buckling of an AMTEC cell wall made of a single sheet of Haynes-25.[9] The results of finite element analyses were compared with the values obtained from compression tests. The analyses consistently overpredicted the buckling load (the load at which buckling commences) by a factor of two to three. The difference between the predictions and the test results were attributed to material imperfections and uncertainties in the test sample dimensions, which were not known and are difficult to incorporate into a finite element analysis model. The results of Ruhkamp et al. indicated the sensitivity of the buckling analysis to small geometric uncertainties or material imperfections.[9]

The objective of this paper is to perform detailed linear stress and buckling analyses of the Nb-1Zr/C-103 cells of El-Genk and King[7] to verify that they will not permanently deform nor buckle during launch, while integrated into a radioisotope generator (Fig. 3). The 16 AMTEC cells in this generator are mounted onto the four side faces of a stack of two general purpose heat source (GPHS) modules (see Fig. 3). Each module produces about 230 or 250 W_{th} at beginning of mission using old or fresh $^{238}PuO_2$ fuel, respectively. The condenser plates of the AMTEC cells are attached to the outer generator housing, which rejects excess heat to space. Details on the design and layout of the generator are given in Fig. 3. The GPHS stack is held in the axial direction by two zirconia/titanium studs placed between the top and bottom of the GPHS stack and the generator housing. In an early generator design the cells served as support members, holding the GPHS stack against the generator housing in the radial direction (see Fig. 3). In such a configuration each cell is preloaded with 223–334 N along its axis.[8] A later version of the generator design incorporated a radial support structure.[10]

The present analyses examined the separate as well as the combined effect of the following on the structural integrity of the cells during launch:

1) A cover gas pressure of ~202 kPa: The radioisotope generator is filled with inert cover gas prior to launch to prevent component oxidation. This cover gas also increases heat dissipation and helps maintain the generator's temperatures within accepted limits.

Received 28 August 2000; revision received 5 January 2001; accepted for publication 24 January 2001.

*Research Assistant, Institute for Space and Nuclear Power Studies, Department of Chemical and Nuclear Engineering. Student Member AIAA.

†Director, Institute for Space and Nuclear Power Studies, and Regents' Professor, Department of Chemical and Nuclear Engineering. Associate Fellow AIAA.

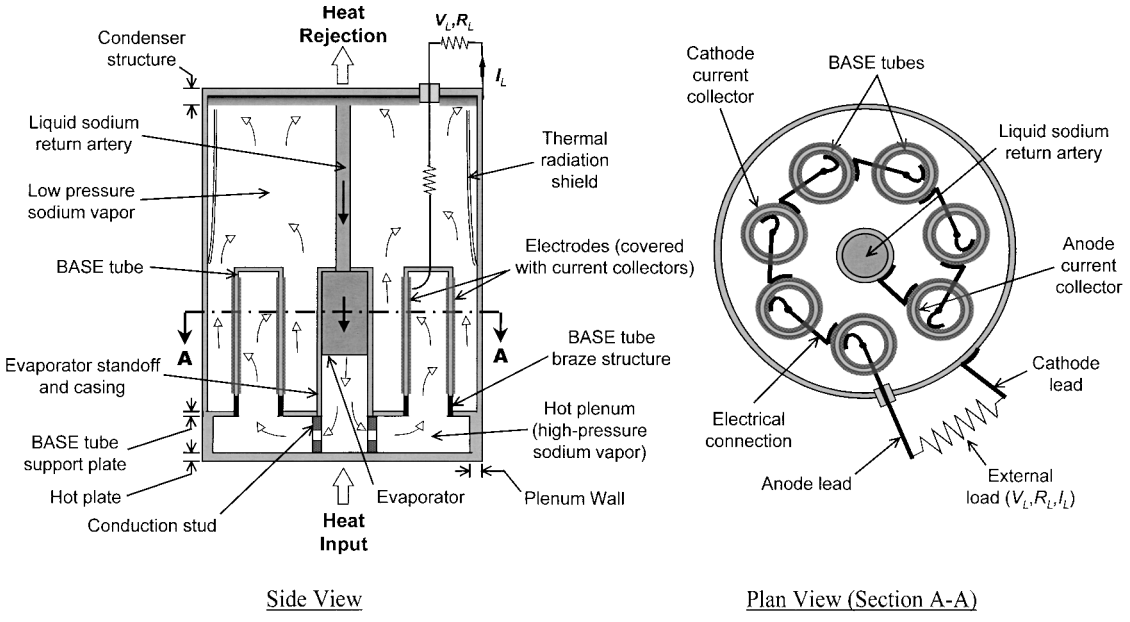

Fig. 1 Cutaway and plane views of a typical multitube, vapor-anode AMTEC cell.

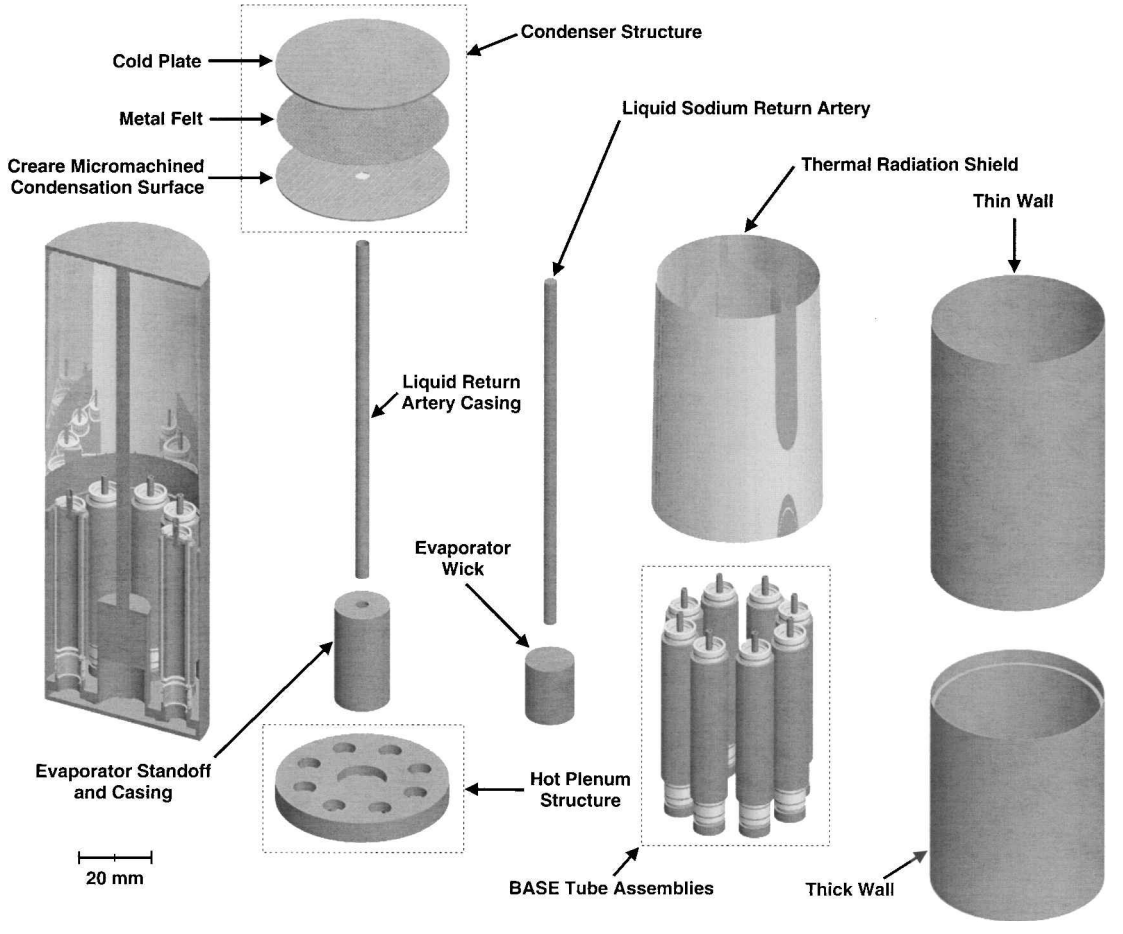

Fig. 2 Exploded trimetric view of a Nb-1Zr/C-103 AMTEC cell.[7]

Following placement in orbit, the cover gas is released, and the interior of the generator equalizes to vacuum.[11]

2) Induced thermal stresses in the cells while operating in the short circuit mode: During launch, the radioisotope generator is operated in the short circuit mode to keep the AMTEC cells relatively cool.

3) Launch accelerations and vibrations: A pseudostatic axial and radial loading of 40 G each is applied to simulate the effects of random vibration and acceleration during launch.[8]

4) A force of 334 N along the axis of each cell: This represents the condition when the cells are used as support members.[8]

The results of the buckling analyses assess the cell design modifications needed to ensure a buckling modifier of at least 3.5 during launch. The buckling modifier is the ratio of the load at which buckling commences to the applied load. The present analyses assume a stress-free reference temperature of 600 K. This temperature is lower than those expected during the actual assembly of the cells,

which are assumed to be above that of the condenser during normal operation.

Stress Analyses

Figure 4 presents a simplified cross-sectional view of the Nb-1Zr/C-103 cell showing the loads considered in the present stress and buckling analyses during launch. Because launch is a relatively short duration event (< 30 min), creep and creep rupture are omitted from consideration. The design stress limit in the present analyses is taken as 98% of the temperature-dependent yield stresses of the structural materials. The stress and buckling analyses are based on the linear static stress and buckling processors in version 12.02 of the commercially available Algor finite element analysis software (http://www.algor.com). Each structural member in the AMTEC cell is assigned a specific group number to identify the structure and specify material properties. Nodal meshes are used to form the computational elements in the stress and buckling analyses models. The nodal operating temperatures are manually added. These temperatures are calculated using the AMTEC Performance Analysis and Evaluation Model (APEAM),[12] with the cell in the short circuit mode of operation. The nodes in the cell's hot plate, pressed against the GPHS modules in the generator, are not allowed to move in the Z direction (along the center axis of the cell). In addition, the center node of the cell condenser is constrained from moving in either the X or the Y directions (along the radius of the cell) to simulate the condition when the condenser plate of the cell is fastened to the generator housing. The material properties used for Nb-1Zr, C-103, BASE, and tantalum[13–19] are summarized in Table 1, and the seven load cases considered in the present stress analyses are detailed in Table 2.

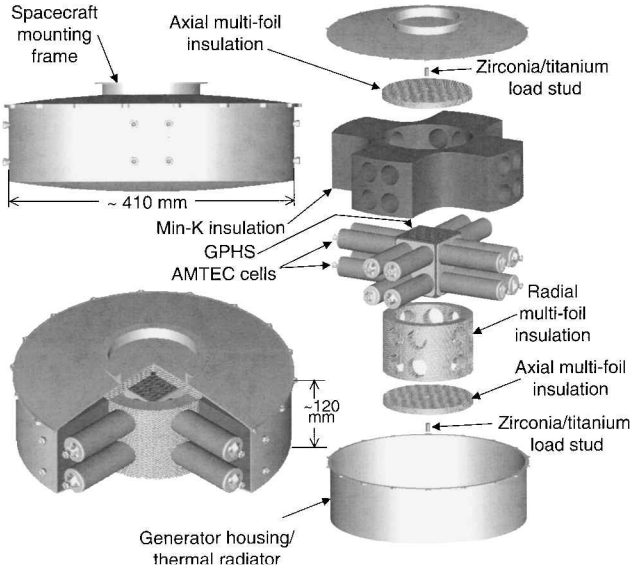

Fig. 3 Exploded isometric view of AMPS radioisotope generator (based on the description by Hendricks et al.[8]).

Stress Analyses Results

Figure 5 displays isometric views of the cell showing the calculated absolute displacements and Von Mises stresses as a result of the load from using the AMTEC cells as structural support members in the generator (load case 1 in Table 2). The induced axial displacement is highest at the condenser, indicating that the cell is compressed against the GPHS stack. The degree of compression, however, is minor, resulting in a displacement of 33 μm or less.

The highest predicted stresses (~27–29 MPa) occur in the thin wall near the condenser and above and below the interface of the thin wall and the thermal radiation shield (Figs. 1 and 5). The Von Mises stresses calculated for the thin wall, constructed of the high-strength niobium alloy C-103, do not exceed 13% of the temperature-dependent yield stress of this material. The small displacements at the condenser, combined with the large margin between the Von Mises stresses and the yield stress, suggest that using the cells as structural support members in the generator does not pose a challenge to their structural integrity. Figure 5 shows a low stress region at the line of attachment of the thermal radiation shield to the thin wall, above the BASE tubes. Along the line of attachment, the thermal radiation shield provides some support to the cell wall, resulting in a lower local stress.

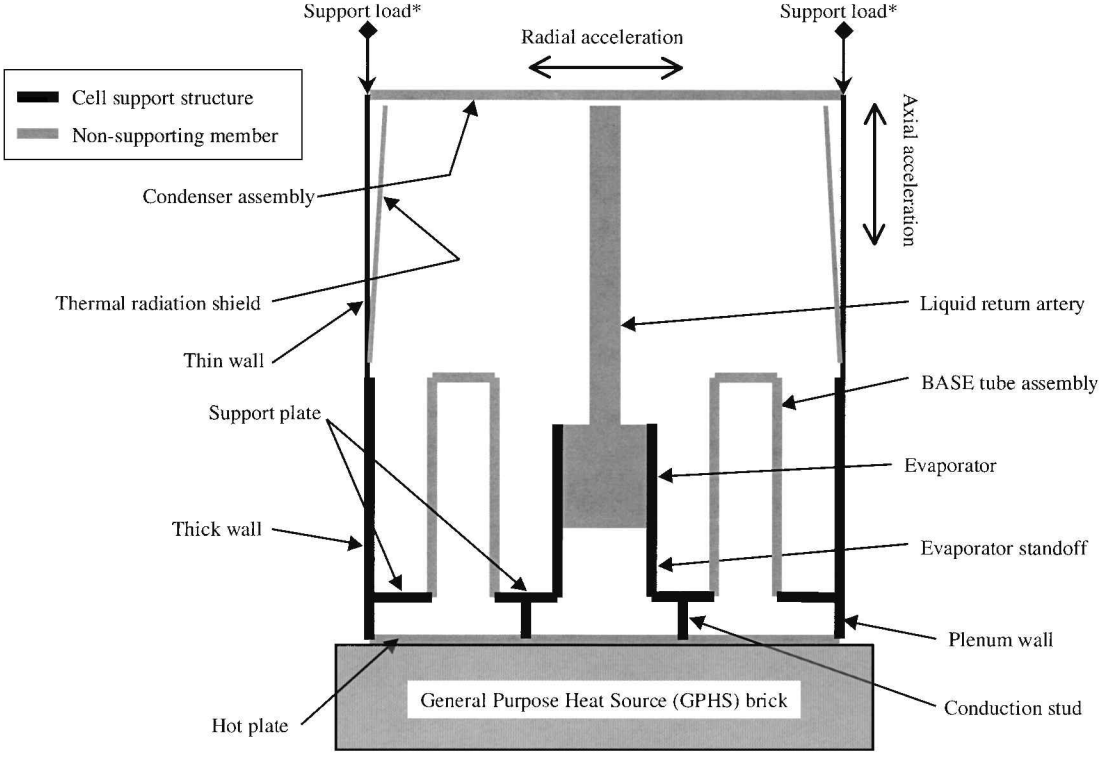

* Present if the AMTEC cell is used to provide support for the GPHS, which is investigated in the present analysis

Fig. 4 Illustration of the applied loads on a Nb-1Zr/C-103 AMTEC cell during launch.

Table 1 Material properties used in the present linear stress and buckling analyses[13–19]

Property	Temperature, K							
	500	600	700	800	900	1000	1100	1200
a) Nb-1Zr (Nb-1% Zr)								
Density,[13] kg/cm^3					8,580			
Poisson' ratio[14]					0.32			
Elastic modulus,[13] GPa	76	74	73	71	68	66	62	56
Linear thermal expansion coefficient,[15] $K^{-1} \times 10^6$	7.60	7.80	8.00	8.20	8.30	8.40	8.50	8.60
Yield strength,[16] MPa	149	143	137	132	127	122	118	114
b) C-103 (Nb-10% Hf-1% Ti-0.5%Zr)								
Density,[13] kg/cm^3					8,860			
Poisson' ratio[14]					0.32			
Elastic modulus,[13] GPa	85	83	81	79	78	75	73	70
Linear thermal expansion coefficient,[15a] $K^{-1} \times 10^6$	7.80	8.00	8.10	8.20	8.40	8.60	8.70	8.80
Yield strength,[13] MPa	304	283	263	242	222	201	181	160
c) Tantalum								
Density,[5] kg/cm^3					16,650			
Poisson' ratio[14]					0.35			
Elastic modulus,[13] GPa	181	180	178	177	176	174	173	172[b]
Linear thermal expansion coefficient,[15] $K^{-1} \times 10^6$	6.80	6.90	7.10	7.20	7.20	7.30	7.35	7.40
Yield strength,[13] MPa	241	201	172	150	134	119	108	98
d) BASE								
Density,[17] kg/cm^3					3,260			
Poisson' ratio[17]					0.265			
Elastic modulus,[17] GPa					203			
Linear thermal expansion coefficient,[18] $K^{-1} \times 10^6$	3.38	2.97	2.99	3.45	4.34	5.67	7.43	9.62
Fracture strength,[19] MPa					90			

[a]Assumed equal to pure niobium. [b]Extrapolated.

Table 2 Stress analysis cases performed for the Nb-1Zr/C-103 AMTEC cell[7]

Case	Description	Applied loads
1	Structural support load	334 N parallel to the cell's center axis 202 kPa cover gas pressure
2	Pressure loads	60 kPa anode sodium vapor pressure 30 Pa cathode sodium vapor pressure
3	Thermal stresses	Short circuit temperature profile
4a	Axial acceleration and vibration	40 G applied axially
4b	Radial acceleration and vibration	40 G applied radially
5a	Combined axial load	All loads from cases 1,2,3, and 4a
5b	Combined radial load	All loads from cases 1,2,3, and 4b

The calculated Von Mises stresses in load case 2 (Table 2) are concentrated at the same locations as in the preceding load case. The displacements, however, are significantly different, indicating that the cell is compressed in the radial direction with little variation in the displacements along its length. The Von Mises stresses resulting from the cover gas pressure loading (~43–45 MPa) are more significant than those resulting from the support load, but do not exceed 20% of the yield stresses of C-103. The absolute displacements are also insignificant (less than 50 μm at the point of maximum deflection at the center of the condenser). These displacements and the Von Mises stresses are expected to disappear once the generator is deployed into orbit and the cover gas is vented into space.

In load case 3 the induced thermal stresses in the evaporator wick, in the evaporator standoff, and in the BASE tube assemblies are significant. The highest thermal stresses (~98 MPa) occur near the bottom end of the evaporator wick, at the interface with the evaporator standoff. The thermal stresses in the BASE tube assemblies are also significant, particularly in the BASE braze (~82 MPa) and at the top cap of the BASE tubes (~71 MPa). The displacements resulting from the thermal expansion of various structural members of the cell are mainly in the axial direction, resulting in the displacement of the condenser plate by as much as 337 μm away from the support plate.

The calculated Von Mises stresses in the BASE tube may exceed the fracture strength of BASE[19]; however, the present linear static stress analyses do not adequately represent the complexity of the BASE tube assemblies and are likely to overestimate the thermal stresses. The BASE assembly is a complex, multicomponent structure that readily conducts heat, electrically insulates the BASE from the support plate, and withstands induced differential thermal expansion. The simplified BASE assembly used in the current stress analysis provides good information about the stress transmission from the BASE assembly to the support plate; however, the simplified BASE assembly does not provide accommodation for thermal expansion, and thus the calculations overestimate the induced thermal stresses. Therefore, more detailed modeling and analysis of the BASE tube assemblies is recommended to qualify the cells for launch.

In addition, the present linear static stress model does not account for the slip joint between the evaporator standoff and evaporator wick, which would relieve some of the calculated thermal stresses at that interface. However, because the calculations show that the current worst-case stresses in the evaporator standoff do not exceed 77% of the temperature-dependent yield stress of Nb-1Zr, the evaporator assembly is unlikely to experience any permanent deformation during launch.

In load case 4a axial acceleration of the cell results in limited concentrations of Von Mises stresses (Fig. 6) within the conduction stud and at the BASE braze/support plate interface. These stresses, however, do not exceed 11% of the yield strengths of the materials at those locations. The displacements from the axial acceleration loading, present mainly in the condenser assembly, do not exceed 25 μm.

The effect of the radial acceleration loading (load case 4b) is more significant (see Fig. 7). Minor Von Mises stress concentrations develop at the center of the condenser assembly and in the lower portion of the thin wall. These stresses do not exceed 16% of the materials' yield stresses. The cantilevered support of the BASE tube assemblies by the support plate results in Von Mises stresses of up to 80% of the yield stresses of the materials of the support plate and of the BASE braze segment. These stresses are a consequence of the single-ended support of the relatively heavy BASE tube assemblies. When the BASE tube assemblies are subjected to acceleration parallel to the support plate, a bending moment results. This bending moment also causes a deflection at the top of the BASE assemblies of up to 274 μm. This deflection is expected to disappear

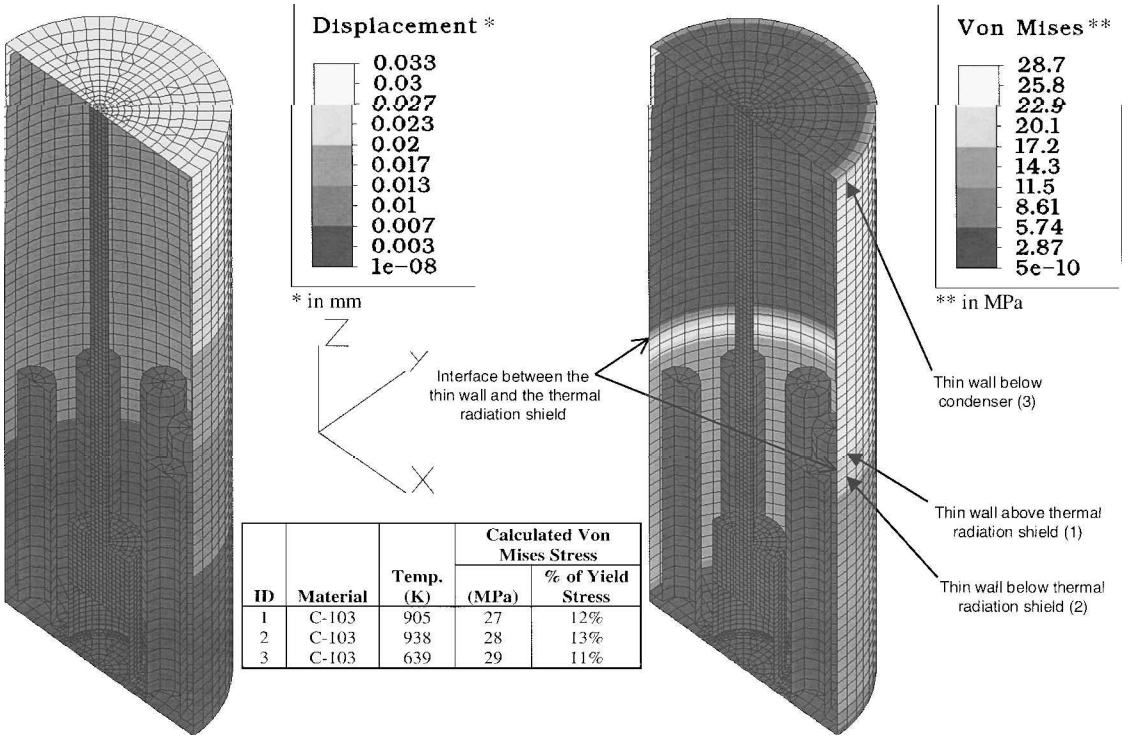

ID	Material	Temp. (K)	Calculated Von Mises Stress (MPa)	Calculated Von Mises Stress % of Yield Stress
1	C-103	905	27	12%
2	C-103	938	28	13%
3	C-103	639	29	11%

Fig. 5 Predicted absolute displacements and Von Mises stresses resulting from a structural support load of 334 N.

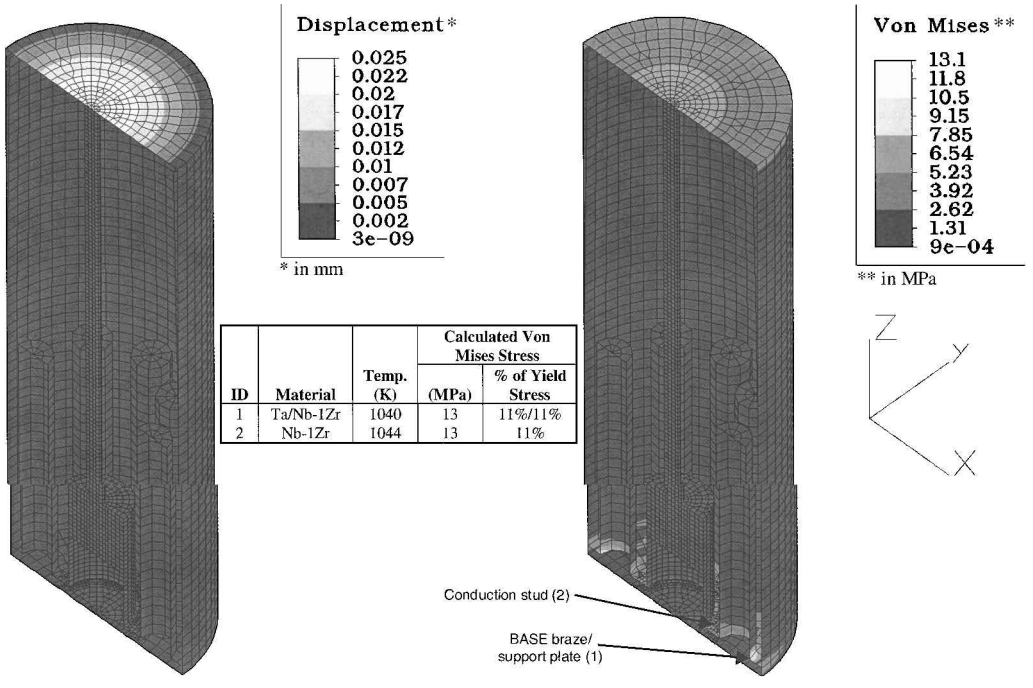

ID	Material	Temp. (K)	Calculated Von Mises Stress (MPa)	Calculated Von Mises Stress % of Yield Stress
1	Ta/Nb-1Zr	1040	13	11%/11%
2	Nb-1Zr	1044	13	11%

Fig. 6 Predicted absolute displacements and Von Mises stresses resulting from an axial acceleration of 40 G.

at the completion of launch, as long as the total induced Von Mises stresses in the BASE assembly and the support plate do not exceed the materials' yield stresses.

The results of the combined loading with axial (load case 5a) and radial acceleration (load case 5b) are shown in Figs. 8 and 9, respectively. In the combined loading case with axial acceleration (Fig. 8), the displacements, primarily in the axial direction, are highest at the condenser end of the cell. Excluding the stresses in the evaporator and the BASE tube assemblies, the highest Von Mises stresses, at the top and bottom of the thin wall, do not exceed 21% of the yield stresses in these locations. The induced Von Mises stresses in the evaporator structures do not exceed 77% of the yield stress of Nb-1Zr, suggesting that these structures are unlikely to experience permanent deformation during launch.

Under the combined loading with radial acceleration (Fig. 9), the highest displacement occurs along one edge of the condenser and at the top of three of the BASE tube assemblies. The highest Von Mises stresses at the interface between the BASE tube assemblies and the support plate are less than 86% of the yield stress of the materials at those locations. Von Mises stresses of up to 34% of the yield stress are induced at the triple interface between the support plate, the plenum wall, and the thick portion of the wall. The total

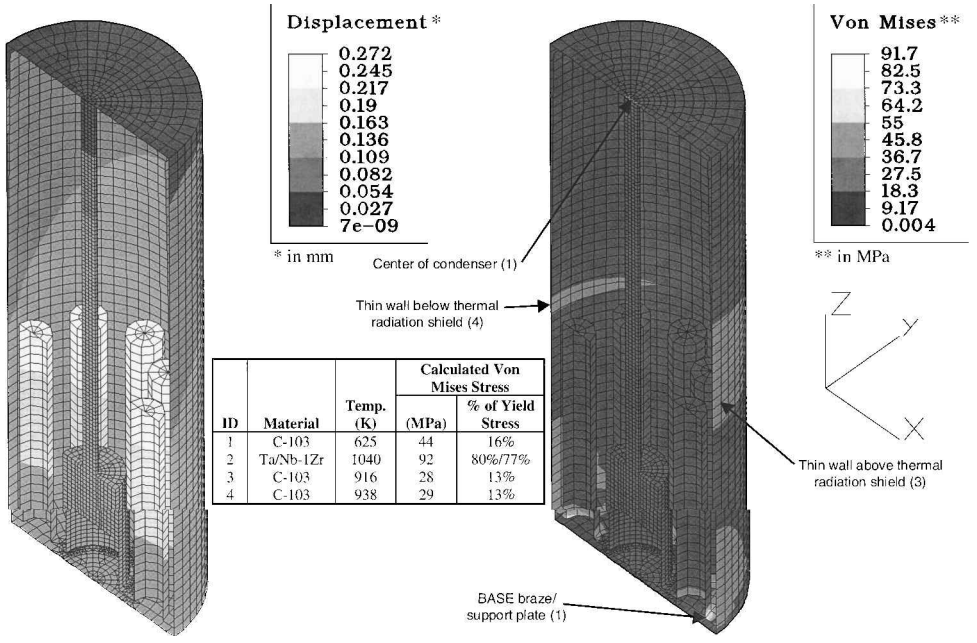

ID	Material	Temp. (K)	Calculated Von Mises Stress (MPa)	% of Yield Stress
1	C-103	625	44	16%
2	Ta/Nb-1Zr	1040	92	80%/77%
3	C-103	916	28	13%
4	C-103	938	29	13%

Fig. 7 Predicted absolute displacements and Von Mises stresses resulting from a radial acceleration of 40 G.

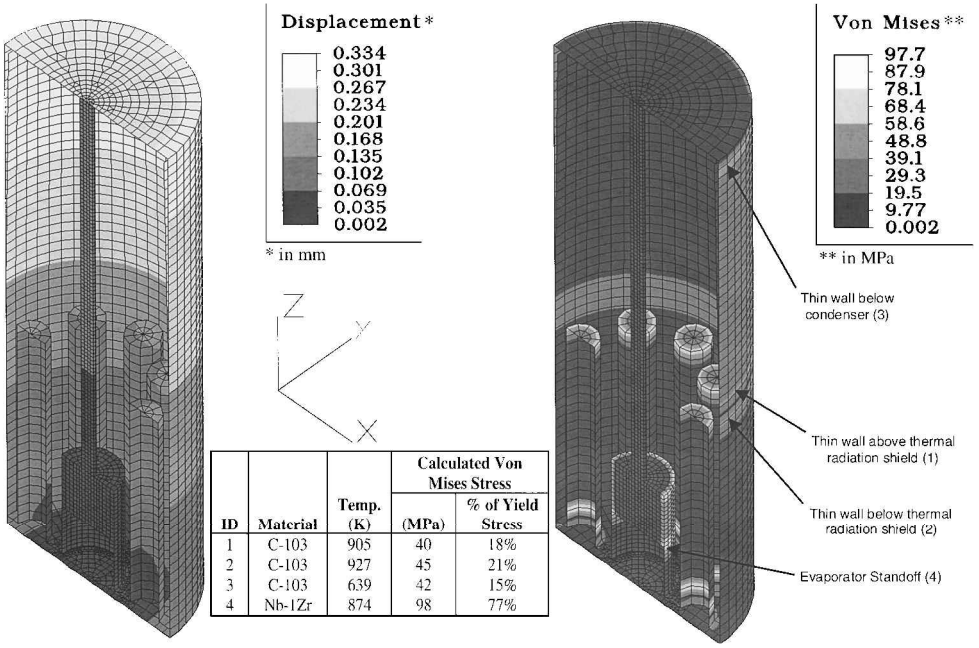

ID	Material	Temp. (K)	Calculated Von Mises Stress (MPa)	% of Yield Stress
1	C-103	905	40	18%
2	C-103	927	45	21%
3	C-103	639	42	15%
4	Nb-1Zr	874	98	77%

Fig. 8 Predicted absolute displacements and Von Mises stresses resulting from combined loading with axial acceleration.

induced stresses in the evaporator assembly do not exceed 77% of the yield stress of Nb-1Zr.

The total Von Mises stresses in the combined load cases (Figs. 8 and 9) do not exceed 86% of the yield stress at any point in the cell structures investigated. However, the geometric stability of the cell under load needs to be verified to ensure that it will not buckle during launch. The next section describes the results of the buckling analyses.

Buckling Analyses Results

Owing to the current limitations of the Algor buckling analysis processor, it was not possible to include the conduction stud, the evaporator assembly, and the liquid return artery in the buckling model. Instead, appropriate boundary conditions or nodal forces are used to account for these elements. Nodal forces at the support plate/evaporator standoff interface, equivalent to the mass of the evaporator, evaporator standoff, and liquid return artery under 40 G of axial acceleration (40 nodes at 0.212 N/node = 8.48 N total), are applied to account for the evaporator assembly and liquid return artery. The restriction of no axial displacement is applied to the nodes at the support plate/conduction stud interface, emulating the effect of the conduction stud. Restricted displacements are added to the nodes in the hot plate and in the condenser to prevent rotation about the axis of the cell. The rest of the applied loads are the same as in the linear static stress analyses.

The Algor buckling analysis processor provides two important outputs: the buckling modifier and the buckling mode shape. The present analyses use a buckling modifier of 3.5 to provide a conservative margin of safety. The buckling mode shape represents the deformation expected at the beginning of buckling and is useful for determining where buckling is expected to commence

Table 3 Cases of the buckling analysis of the Nb-1Zr/C-103 AMTEC cell[7]

Case	Applied loads	Structural modifications	Calculated buckling modifier
1	334 N parallel to the cell's center axis 40 G axial acceleration 202 kPa external cover gas pressure 60 kPa internal pressure on the anode (hot) side 30 Pa internal pressure on the cathode (cold) side Short circuit temperature profile	None	0.256
2	Same as case 1, without the 334 N load parallel to the cell's center axis	None	0.261
3	Same as case 1, without applied pressures	None	8.883
4	Same as case 1	0.1-mm-thin wall ribs	0.767
5	Same as case 1	0.2-mm-thin wall ribs 0.2-mm-thin wall ribs	1.215
6	Same as case 1	0.1-mm-thick wall ribs 0.3-mm-thin wall ribs	1.550
7	Same as case 1	0.2-mm-thick wall ribs	2.421
8	Same as case 1, reduce cover gas pressure to 150 kPa	0.3-mm-thin wall ribs 0.2-mm-thick wall ribs	3.090
9	Same as case 1, reduce cover gas pressure to 125 kPa	0.3-mm-thin wall ribs 0.2-mm-thick wall ribs	3.557

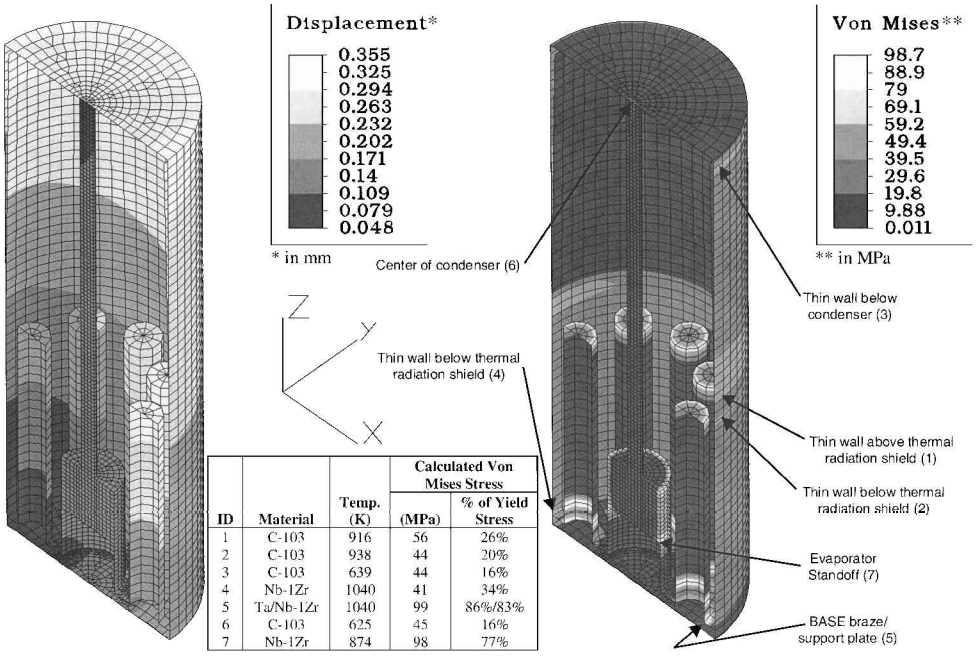

Fig. 9 Predicted absolute displacements and Von Mises stresses resulting from combined loading with radial acceleration.

as well as indicating locations where structural reinforcements are needed.

Table 3 summarizes the nine cases investigated in the present buckling analyses. Figure 10 presents the predicted buckling mode shape for the Nb-1Zr/C-103 in case 1 and shows that buckling begins in the thin (~0.1 mm) portion of the cell wall above the BASE tubes. The thin portion of the wall has crumpled inward, and most of the displacements are in the radial direction. The low buckling modifier for this case (0.256) indicates that buckling could commence at loads roughly one-quarter of those expected during launch.

The small change (<2%) in the buckling modifier between cases 1 and 2 suggests that the 334 N axial force is not a significant contributor to the buckling of the thin portion of the cell wall. The large change in the buckling modifier between cases 1 and 3 (0.256 vs 8.883, respectively), however, demonstrates that the cover gas pressure is a significant contributor to buckling in the thin portion of the cell wall. The shape of the calculated displacements in Fig. 10 indicates that incorporating a number of circumferential reinforcing ribs may strengthen the wall, increasing the buckling modifier.

Cases 4 and 5 in Table 3 examined the effect of adding three circumferential ribs to strengthen the thin (~0.1 mm) portion of the cell wall, with a pitch-to-width ratio of ~2. In case 4 adding 0.1-mm-thick ribs to strengthen the thin (~0.1-mm-thick) portion of the cell wall increased the buckling modifier from 0.256 to 0.767. Doubling the thickness of the ribs to ~0.2 mm (case 5) increased the critical buckling modifier to 1.215, which is over unity, but below the desired design limit of 3.5. The buckling mode shape for case 5, presented in Fig. 11, shows that buckling now commences in the thick (~0.2 mm) portion of the cell wall facing the BASE tubes, indicating the need for additional structural reinforcement of this part of the wall.

In cases 6 and 7 an additional three circumferential ribs are added to strengthen the thick portion (~0.2 mm) of the cell wall, with a pitch-to-width ratio of ~2.33. In case 6 adding 0.1-mm-thick ribs to the thick portion of the wall increased the buckling modifier slightly, to 1.550. Increasing the thickness of the ribs for both the thick and thin portions of the cell wall by 0.1 mm each (case 7) increases the critical buckling modifier to 2.421.

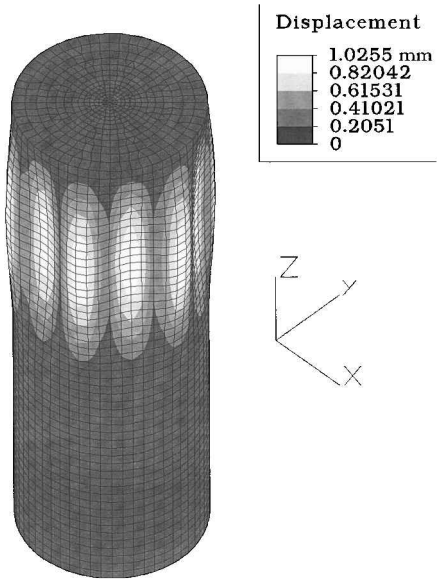

Fig. 10 Predicted buckling mode shape with no design changes (displacements are scaled 2x).

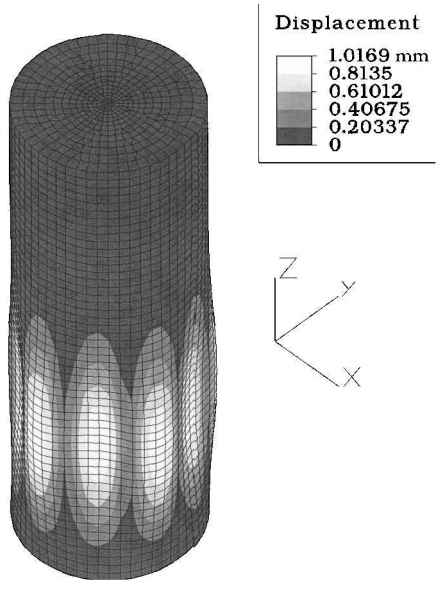

Fig. 11 Predicted buckling mode shape with ribs incorporated into the thin wall above the BASE tubes (displacements are scaled 2x).

Cases 8 and 9 in Table 3 examined the effect of reducing the external cover gas pressure. The cover gas pressure must be greater than one atmosphere (~101 kPa) to prevent the intrusion of air into the generator. In case 8 the external cover gas pressure is reduced from 202 kPa in the base case to 150 kPa, increasing the buckling modifier to 3.090. A further decrease in the cover gas pressure to 125 kPa (case 9) increased the buckling modifier to 3.557, which satisfies the specified design multiplier of 3.5. The buckling mode shape for case 9 (Fig. 12) indicates that the onset of buckling is localized and confined to the thin wall in the regions between ribs. The resulting cell, with three 0.3-mm-thick reinforcing ribs added to the thin cell wall above the BASE tubes and three 0.2-mm-thick reinforcing ribs added to the thick wall facing the BASE tubes, satisfies the design requirements specified for the present analyses—when the cover gas pressure is maintained at or below 125 kPa.

Performance of the Ribbed Nb-1Zr/C-103 Cell

The reinforcing ribs increased the total mass of the Nb-1Zr/C-103 cell by 5.0% (8.1 g) from 163.4 to 171.5 g. The operation envelope of the modified cell is generated using the APEAM developed by the

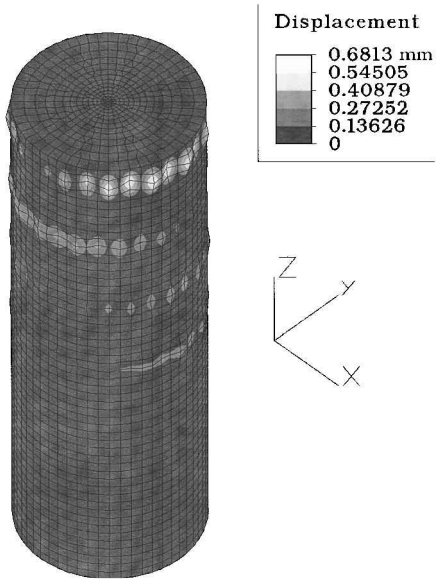

Fig. 12 Predicted buckling mode shape with ribs incorporated into the thick and thin walls (displacements are scaled 2x).

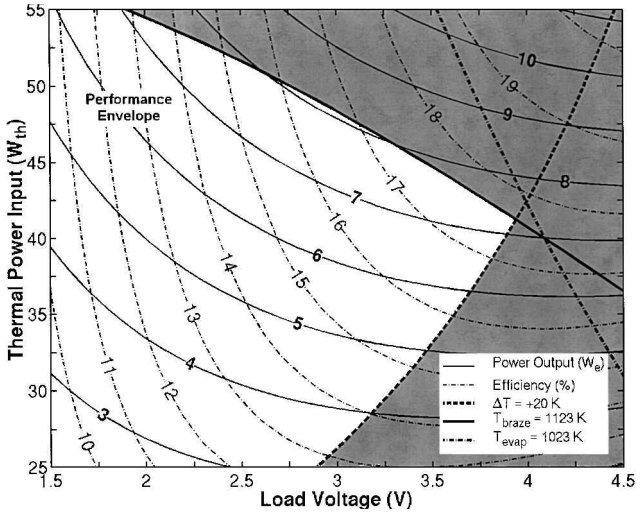

Fig. 13 Performance envelope of the ribbed Nb-1Zr/C-103 cell with advanced electrodes.

Institute for Space and Nuclear Power Studies (see Fig. 13).[12] The white region in Fig. 13 represents the operation envelope in which none of the design temperature limits are exceeded. To prevent the high-pressure sodium from condensing inside the BASE tubes and shorting the cell, the difference between temperature at the cold end of the BASE and the evaporator surface (ΔT) should be at least 20 K. In addition, the temperature of the BASE brazes (T_{braze}) should be maintained below 1123 K to minimize the loss of the volatile elements such as nickel, which would lead to degradation of the brazes and potential leakage of sodium vapor to the low pressure cavity. Also, in order to slow down grain growth and the increase in the size of the pores in the evaporator wick, the evaporator temperature (T_{evap}) should not exceed 1023 K.

The mass and performance of the original and the ribbed cells are compared in Table 4. Using advanced electrodes with $B = 120$ A $K^{1/2}$ Pa m^{-2} and $G = 10$, the maximum voltage of the ribbed cell is 3.9 V at which the electric power output is 7.3 W_e and cell efficiency is 17.6% (Fig. 13). The maximum cell electric power in the operation envelope shown in Fig. 13 is 8.05 W_e, which is 0.05 W_e (or 0.6%) less than that of the original cell. The corresponding load voltage of 3.0 V is the same for both cells, and the ribbed cell's conversion efficiency of 16.7% is 0.6 percentage points (or 3.5%) lower than the original cell. The specific mass of the ribbed cell

Table 4 Comparative performance of the original and ribbed Nb-1Zr/C-103 AMTEC cells

Parameter	Original Nb-1Zr/ C-103 cell[7]	Ribbed Nb-1Zr/ C-103 cell
Overall cell mass	163.4 g	171.5 g
At the maximum electric power output		
Load voltage	3.0 V	3.0 V
Maximum output power	8.3 W_e	8.05 W_e
Efficiency	17.3%	16.7%
Cell specific mass	19.7 g/W_e	21.3 g/W_e
At the maximum load voltage		
Maximum load voltage	4.15 V	3.9 V
Output power	7.1 W_e	7.3 W_e
Efficiency	18.4%	17.6%
Cell specific mass	23.0 g/W_e	23.5 g/W_e

at the maximum electric power increases by 8.1% to 21.3 g/W_e, compared to 19.7 g/W_e for the original Nb-1Zr/C-103 cell without ribs.

Summary and Conclusions

Linear static stress and buckling analyses are performed to investigate whether the Nb-1Zr/C-103 AMTEC cells[7] can survive the loading conditions expected during launch while mounted in a radioisotope generator, without permanent deformation or buckling. During launch, the AMTEC cells in the radioisotope power generator will be subjected to thermal stresses, the pressure of the cover gas in the generator housing, and accelerations and vibrations. If the cells are used as structural support members in the generator, each could be subjected to an additional force of 334 N. The present stress analyses predicted that the induced Von Mises stresses in the structural support members of the Nb-1Zr/C-103 cells[7] would not exceed 86% of the temperature-dependent yield stresses. Results also suggested that there is little apparent penalty for using the AMTEC cells as structural support members in the radioisotope generator.

Buckling analyses of the Nb-1Zr/C-103 cells indicated that, in order to satisfy the buckling modifier of 3.5 desired in the present analyses, it was necessary to incorporate reinforcing ribs into both the thick and thin portions of the cell wall and to decrease the pressure of the inert cover gas in the generator to 125 kPa. The ribbed cell incorporates three 0.3-mm-thick ribs to strengthen the thin (~0.1 mm) portion of the wall above the BASE tubes and three 0.2-mm-thick ribs to strengthen the thick (~0.2 mm) portion of the wall facing the BASE tubes. These ribs are in addition to the thickness of the cell walls and have approximate pitch-to-width ratios of 2.0 and 2.33, respectively. The total mass of the ribbed Nb-1Zr/C-103 cell increased by 5.0% (8.1 g) from 163.4 to 171.5 g. Using advanced electrodes with $B = 120$ A $K^{1/2}$ Pa m^{-2} and $G = 10$, the specific mass of the ribbed cell at the maximum electric power of 8.0 W_e is 21.3 g/W_e, compared to 19.7 g/W_e for the original cell without ribs.

Acknowledgments

This research was sponsored by the University of New Mexico's Institute for Space and Nuclear Power Studies (ISNPS) and supported by the New Mexico Space Grant Consortium. The authors wish to thank Jean-Michel Tournier of ISNPS for his valuable comments as well as his help throughout the course of this research.

References

[1]Merrill, J., Schuller, M., Sievers, M., Borkowski, C., Huang, L., and El-Genk, M., "Vacuum Testing of High Efficiency Multi-Base Tube AMTEC Cells," *Proceedings of the 32nd Intersociety Energy Conversion Engineering Conference*, Inst. of Electric and Electronics Engineers, Piscataway, NJ, Vol. 2, 1997, pp. 1184–1189.

[2]Merrill, J., Schuller, M., and Huang, L., "Vacuum Testing of High-Efficiency Multitube AMTEC Cells: February 1997-October 1997," *Proceedings of the Space Technology and Applications International Forum (STAIF-98)*, edited by M. S. El-Genk, AIP Conference Proceedings 420, American Inst. of Physics, New York, 1998, pp. 1613–1620.

[3]Merrill, J., and Mayberry, C., "Experimental Investigation of Multi-AMTEC Cell Ground Demonstration Converter Systems Based on PX-3 and PX-5 Series AMTEC Cells," *Proceedings of the Space Technology and Application International Forum (STAIF-99)*, edited by M. S. El-Genk, AIP Conference Proceedings 458, American Inst. of Physics, New York, 1999, pp. 1369–1377.

[4]El-Genk, M. S., Tournier, J.-M., James, R., and Mayberry, C., "Super-Alloy, AMTEC Cells for the Pluto/Express Mission," *Proceedings of the Space Technology and Application International Forum (STAIF-99)*, edited by M. S. El-Genk, AIP Conference Proceedings 458, American Inst. of Physics, New York, 1999, pp. 1293–1300.

[5]King, J. C., and El-Genk, M. S., "Review and Selection of Refractory Materials for AMTEC Cells in Space Power Applications," *Journal of Propulsion and Power*, Vol. 17, No. 3, 2001, pp. 545–554.

[6]Hendricks, T., Huang, C., and Huang, L., "AMTEC Cell Optimization for Advanced Radioisotope Power System (ARPS) Design," *Proceedings of the 34th Intersociety Energy Conversion Engineering Conference*, [CD-Rom Paper 1999-01-2655], Society of Automotive Engineers, Inc., Warrendale, PA, 1999.

[7]El-Genk, M. S., and King, J. C., "Performance Analyses of a Nb-1Zr/C-103, Vapor Anode, Multi-Tube AMTEC Cell," *Journal of Energy Conversion and Management*, Vol. 42, No. 6, 2001, pp. 721–739.

[8]Hendricks, T. J., Huang, C., and Sievers, R. K., "AMTEC Radioisotope Power System Design and Analysis for Pluto Express Fly-By," *Proceedings of the 32nd Intersociety Energy Conversion Engineering Conference*, Inst. of Electric and Electronics Engineers, Piscataway, NJ, Vol. 1, 1997, pp. 501–508.

[9]Ruhkamp, J. D., McDougal, J. R., and Kramer, D. P., "Finite Element Analysis of ARPS Structures," *Proceedings of the 33rd Intersociety Energy Conversion Engineering Conference*, [CD-ROM Paper 98-393], American Nuclear Society, LaGrange Park, IL, 1998.

[10]Hendricks, T. J., and Huang, C., "System Design Impacts of Optimization of the Advanced Radioisotope Power System (ARPS) AMTEC Cell," *Proceedings of the 33rd Intersociety Energy Conversion Engineering Conference*, [CD-ROM Paper 98-407], American Nuclear Society, LaGrange Park, IL, 1998.

[11]Bennett, G. L., Lombardo, J. J., Hemler, R. J., and Peterson, J. R., "The General-Purpose Heat Source Radioisotope Thermoelectric Generator: Power for the Galileo and Ulysses Missions," *Proceedings of the 21st Intersociety Energy Conversion Engineering Conference*, American Chemical Society, Washington, DC, Vol. 3, 1986, pp. 1999–2011.

[12]Tournier, J.-M., and El-Genk, M. S., "Performance Analysis of Pluto/Express, Multitube AMTEC Cells," *Journal of Energy Conversion and Management*, Vol. 40, No. 2, 1999, pp. 139–173.

[13]Tietz, T. E., and Wilson, J. W., *Behavior and Properties of Refractory Metals*, Stanford Univ. Press, Stanford, CA, 1965, pp. 28–39, 377–409.

[14]Wilkinson, W. D., *Properties of Refractory Metals*, Gordon and Breach, New York, 1969, pp. 29–138.

[15]Touloukian, Y. S., Kirby, R. K., Taylor, R. E., and Desai, P. D., *Thermophysical Properties of Matter, the TPRC Data Series*, Vol. 12, IFI/Plenum, New York, 1970, pp. 236–243, 316–322, 958–961.

[16]Condliff, A. F., and Marsh, R. J., "Selection of Structural Materials for Space Nuclear Power Generators," *Space Nuclear Power Systems 1986*, edited by M. S. El-Genk and M. D. Hoover, Orbit, Malabar, FL, 1987, pp. 275–281.

[17]McDonough, W. J., Flinn, D. R., Stern, K. H., and Rice, R. W., "Hot Pressing and Physical Properties of Na Beta Alumina," *Journal of Materials Science*, Vol. 13, No. 11, 1978, pp. 2403–2412.

[18]Ryan, M. A., Williams, R. M., Allevato, C. E., Vining, C. B., Lowe-Ma, C. K., and Robie, S. B., "Thermophysical Properties of Sodium β"-Alumina Polycrystalline Ceramic," *Journal of Physics and Chemistry of Solids*, Vol. 55, No. 11, 1994, pp. 1255–1260.

[19]Virkar, A. V., and Gordon, R. S., "Fracture Properties of Polycrystalline Lithia-Stabilized β''-Alumina," *Journal of the American Ceramic Society*, Vol. 60, No. 1–2, 1977, pp. 58–61.